Measured and simulated time-evolution PD characteristics of typical installation defects in MV XLPE cable terminations

E. N. N. Haikali and C. Nyamupangedengu

Abstract— **In condition monitoring of medium voltage (MV) power cable accessories, there are still challenges in the recognition of partial discharge (PD) defects. In the present paper, typical installation defects were deliberately introduced into MV XLPE power cable terminations. Accelerated ageing under PD activity was achieved by applying voltage at elevated frequency for 900 hours. At suitable time intervals, off-line PD measurements were conducted for each test specimen at 50 Hz test voltage. The results show that the initial PD signatures in the form of Partial Discharge Phase-Resolved-Patterns (PDPRP) are unique for each defect type. The signatures in turn evolve uniquely under continuous voltage application. A modified 3-Capacitor PD model based on the physiochemical processes in the discharge area was implemented in MATLAB Simulink™. The measured initial PD characteristics and the subsequent time-dependent changes were interpreted by comparison with the computer numerical simulation results. It is confirmed that the conductivity of the discharging surface area as well as the voltage at which the cavity breaks down, both change with ageing under PD activity, are the dominant parameters that influence the time-evolution of the PD signatures. Furthermore, the geometry and ventilation of the discharge area is a function of the installation defect type and therefore each defect type gives a unique PD signature. The ability to recognise installation defect through PD tests immediately after installation as well as during the course of on-line PD monitoring is desirable in condition monitoring of power cables. The findings strengthen the credibility of PD diagnosis as an after-installation test as well as in-service condition monitoring technique of MV power cable terminations.**

Index Terms—**Cable terminations, Partial discharges, Time-evolution, PD model**

I. Introduction

PARTIAL discharge (PD) diagnosis is now a widely accepted insulation condition assessment technique. However, its application in distribution power cables may not be at the same scale as in higher voltage systems. In the advent of the evolution of electrical power grids in response to the increasing integration with distributed generation and the concept of smart grids [1], the corresponding maintenance engineering philosophy in distribution systems is changing. The required reliability levels inevitably become stricter in smart power distribution systems. Continuous condition monitoring has become one of the important techniques in condition-based maintenance which in-turn is a characteristic feature of modern effective asset management practice [2, 3, 4].

In medium voltage power cable installations and especially in South Africa, the cable accessories (terminations and joints) are assembled/constructed on the installation site. Often the installations are carried out under emergency and unfavourable conditions such as power supplies restoration after a cable fault or in hash mining operations environment. It has been established that most faults in MV XLPE power cables are attributed to poor workmanship in the stripping and assembling of the various layers of material in the accessory [2]. The installation defects are often not detected through the standardised conventional after-installation tests for MV XLPE power cables [5], and therefore eventually cause the cables to fail prematurely. It is therefore desired to detect the installation defects as early as possible and take corrective measures. In the literature, there have been efforts towards developing better understanding of PD characteristics of installation defects in MV XLPE power cable accessories [6].

In our previous work, the initial partial discharge signatures of typical defects in MV XLPE cable terminations were studied and found to exhibit distinct defect-type dependent features [7]. The present work further extends the investigation by studying how the partial discharge behaviour of the typical installation defects evolve with time under continuous PD activity. The obtained physical experimental measurement results are analysed and validated through comparison with results from a mathematical model that is implemented in a computer simulation platform.

II. The Experimental Work

The experimental work entailed cable termination specimens' preparation where specific defects were deliberately introduced in each core of the 3-core XLPE cable samples. The test specimens were then subjected to continuous PD-induced ageing at a suitable voltage above the PD inception voltage but at elevated frequency to accelerate the ageing process.

E. N. N. Haikali is with the NamPower utility in Namibia and also currently completing MSc Engineering research work at the Universityof the Witwatersrand, Johannesburg. (e-mail: ennhaikali@gmail.com). C. Nyamupangedengu is an associate professor of high voltage engineering in the School of Electrical & Information Engineering at the University of the Witwatersrand, Johannesburg, South Africa (e-mail: cuthbert.nyamupangedengu@wits.ac.za).

Based on *"The unique PD signatures of artificial installation defects introduced in MV XLPE power cable terminations"*, by E. Haikali and C. Nyamupangedengu which appeared in the Proceedings of Southern African Universities Power Engineering Conference (SAUPEC) 2018, Johannesburg, 24 to 26 January.

Defect type	Geometry
Ring-cut: V-shaped air-filled circular canal; • 1 mm deep, 0.6 mm wide (core 1&2) • 2 mm deep, 0,8 mm wide (core 3)	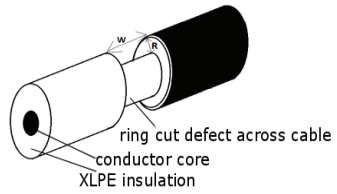
Tramline: V-shaped air-filled longitudinal canal; • 1 mm deep, 0.4 mm wide (core 1&2) • 2 mm deep, 0,8 mm wide (core 3)	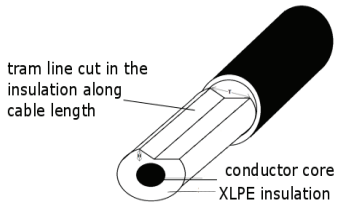
Semicon feather: Triangular shape protrusion of semicon on insulation surface; • 10 mm base, 12 mm height (core 1&2) • 5 mm base, 12.5 mm height (core 3)	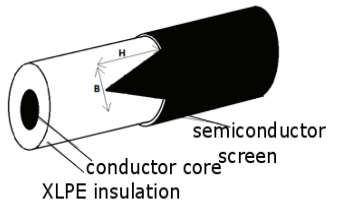

Fig. 1. The artificial defects introduced in the MV XLPE cable terminations

At appropriate intervals, PD measurements were conducted off-line at 50 Hz for each cable core after which the cables would continue to be simultaneously aged. The following sections present the details of the test specimens and test the test procedure.

A. Test Samples Preparation

The common installation defects in MV XLPE power cables investigated in the present work are those due to poor skills in stripping the semiconductor layer resulting in cuts into the insulation as well as causing non-uniform edges of the semiconducting layer. Based on the geometries, the defects have been termed; tramline, ring-cut and semicon feather. More details of the defects are in [7] and Fig. 1 summarizes the geometries of the defects.

Each test specimen was 1-meter-long, 3-core 6.6/11 kV XLPE cable. On one end of the cable, each core was stripped and terminated with defect-free heat shrink accessories. On the other end, each of the two cores (core 1 & 2) had identical defects introduced before applying the heat shrink termination material, and this was for repeatability validation. A more severe defect but of the same type as in cores 1 and 2 was introduced in core 3 before installing the heat shrink termination. Inclusion of the more severe defect in the study was to check on the influence of defect size on the PD behaviour.

The three cable samples, each with three defected cores were subjected to accelerated exposure to PD activity as explained in the next section. Included in the test rig was a 1-meter long 3-core cable sample with defect-free terminations on both ends that was used as a control test specimen.

B. Accelerated PD Ageing Procedure and the PD Signal Measurements

A test voltage of 16 kV_{rms} at 350 Hz was applied to the test specimens connected in parallel in a test rig for 8 hours in accordance with the procedure depicted in Fig. 2. The choice of 350 Hz as accelerated ageing supply voltage frequency was based on the need to increase the rate of PD-induced ageing while keeping within the range of the supply voltage frequency that causes the same effect on insulation as the power frequency. Mazzanti et al. [8] have reported that the effect of frequency on the ageing of insulation is linear up to 400 Hz while Mashikani et al. [9] found it to be up to 600 Hz [10]. Bartnikas at al. [11] however observed similar ageing mechanisms at supply voltage frequencies up to 1 kHz in solid polymer insulation. It can therefore be argued that the elevated frequencies have the same effect on the insulation as that of power frequency (50 Hz or 60 Hz), but cause accelerated PD-induced ageing due to increased voltage cycles.

After every 8 hours of ageing, each cable core was taken through PD measurements using the setup shown in Fig. 3 and procedure as in Fig. 4. The sequence of continuous ageing for 8 hours followed by off-line PD measurements at 50 Hz test voltage for each core and back to continuous ageing was repeated until 900 hours of cumulative ageing.

The PD measurements were conducted on one core at a time while the other two cores would be connected to ground as shown in Fig. 3. Corona rings were fitted onto the conductor ends of each core to prevent corona that would interfere with the genuine PD signals. The tests were conducted in a double shielded high voltage laboratory with average noise base in the order of 0.4 pC.

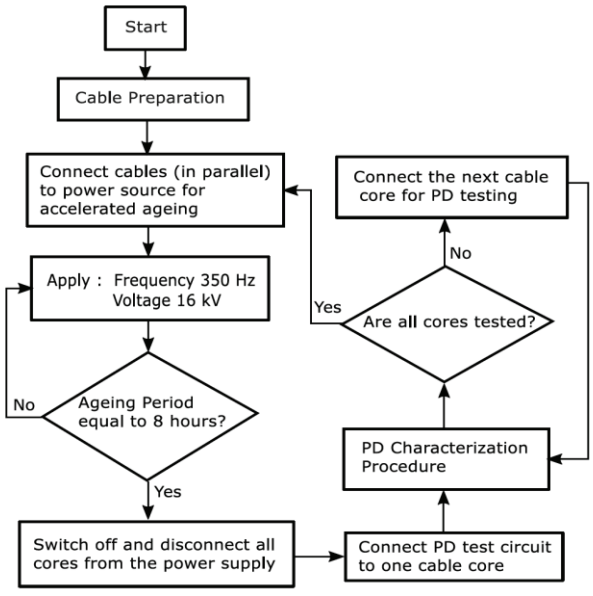

Fig. 2. The accelerated PD ageing protocol

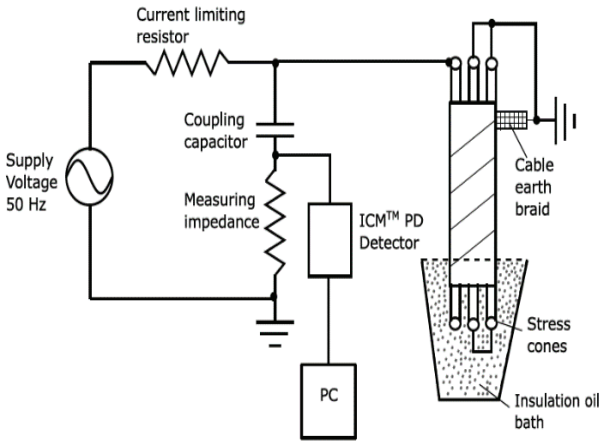

Fig. 3. The PD measurement setup [12]

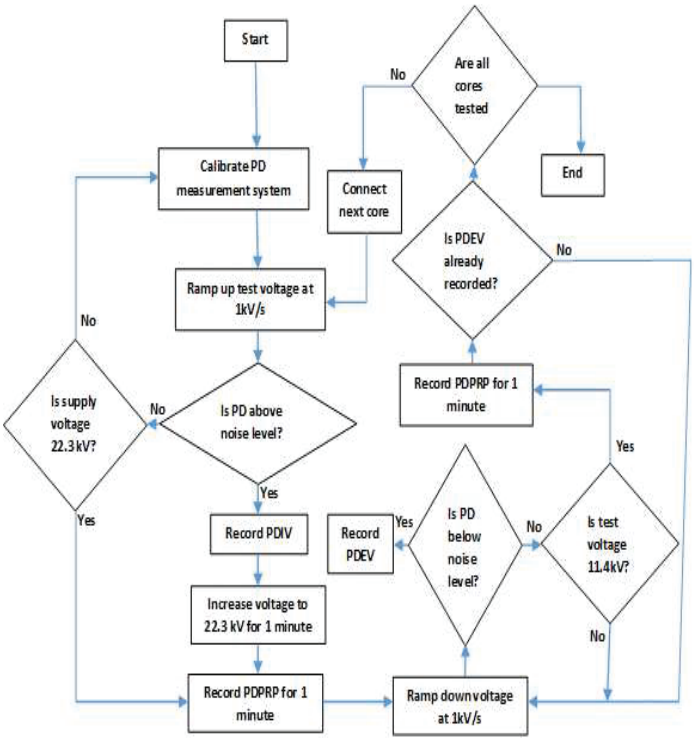

Fig. 4. The PD measurement protocol throughout the accelerated ageing process

Using a Power Diagnostix ICMcompact™ equipment, the PDIV (Partial Discharge Inception Voltage), PDPRP, Maximum PD apparent charge (Q_{max}) and PD pulse repetition rate (PDPRR) were recorded at intervals throughout the 900 hours of accelerated ageing of the test specimens. The experimental results are presented and discussed in the next section.

C. *PD Measurement Results and Discussion*

Ring-cut PD defect: The PDIV, apparent charge magnitude (Q_{max}) and PDPRR throughout the 900-hour ageing period are plotted in Fig. 5. The corresponding typical PDPRP in the identified ageing stages are presented in Fig. 6.

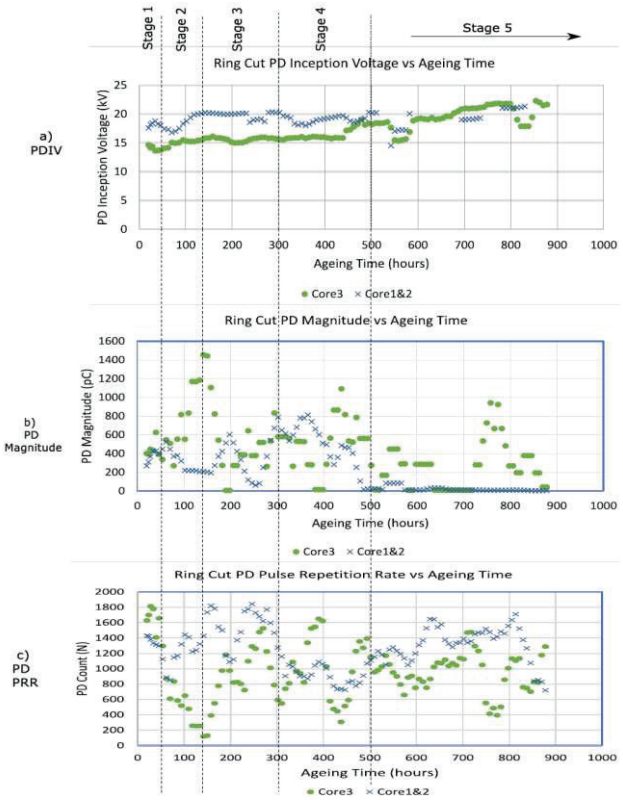

Fig. 5. The ring-cut defect PDIV, Q_{max} and PDPRR evolution

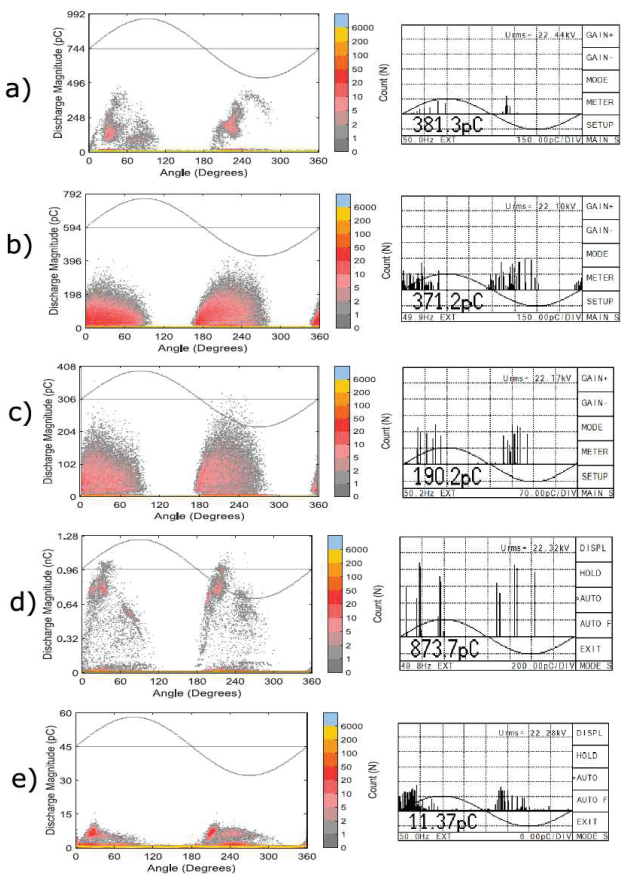

Fig. 6. Ring-cut defect PDPRP changes with time of voltage application; a, b, c, d and e correspond to ageing stages 1, 2, 3, 4, and 5 depicted in Fig. 5.

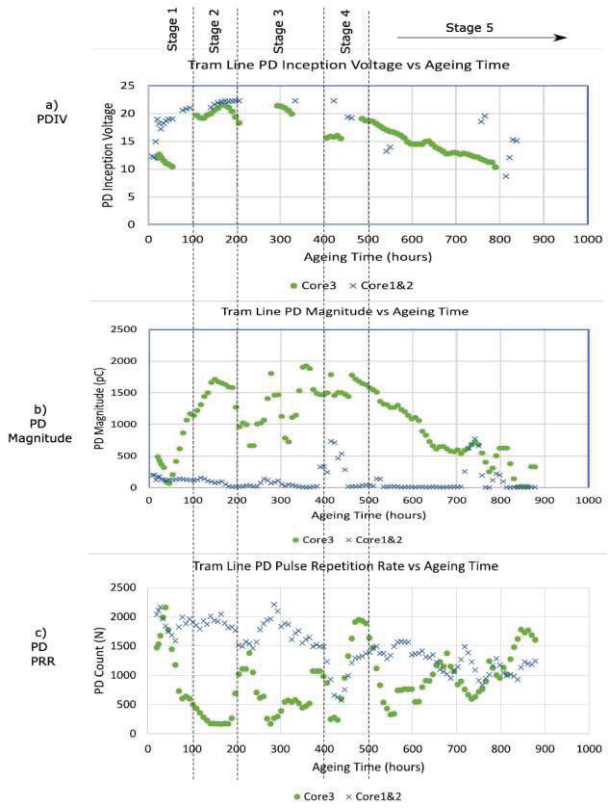

Fig. 7. Tramline defect PDIV, Q_{max} and PDPRR evolution

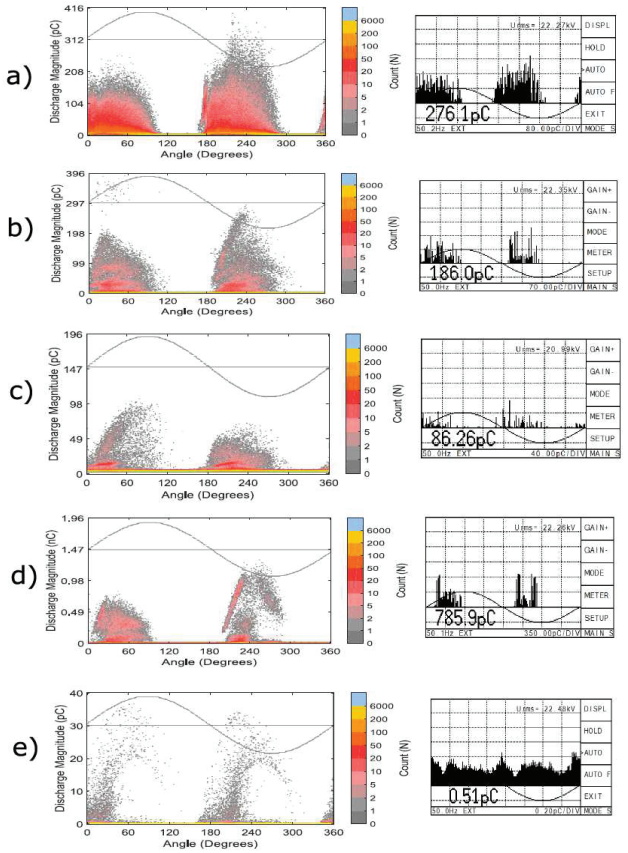

Fig. 8. Tramline defect PDPRP changes with time of voltage application; a, b, c, d and e correspond to ageing stages 1, 2, 3, 4, and 5 depicted in Fig. 7.

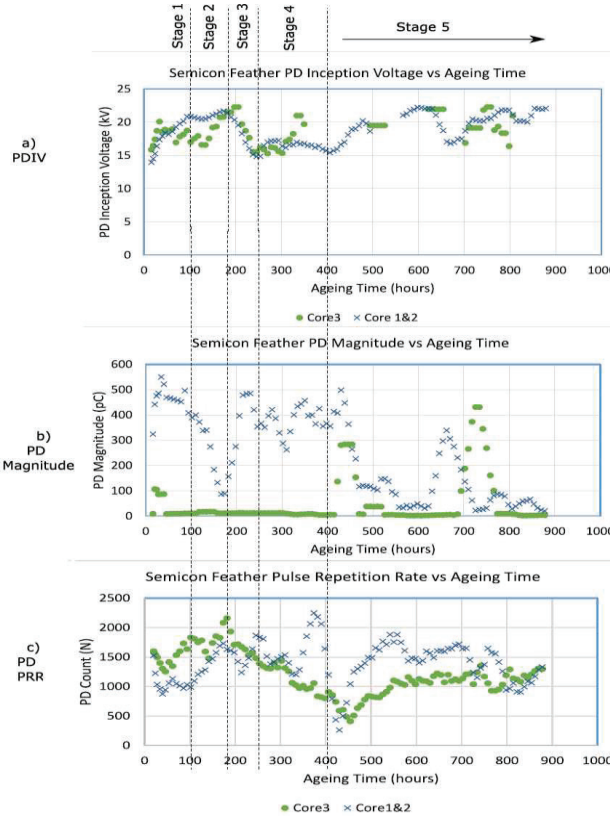

Fig. 9. Semicon defect PDIV, Q_{max} and PDPRR evolution

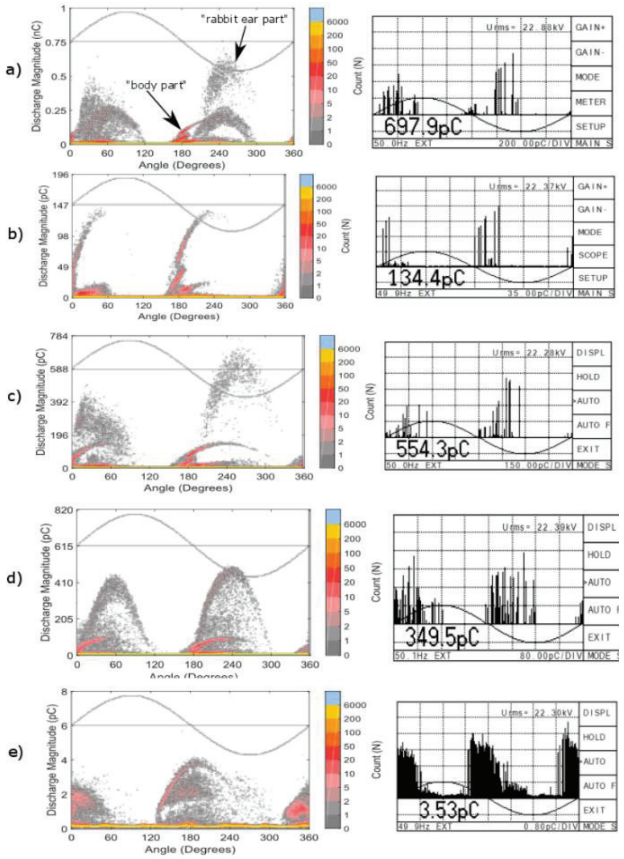

Fig. 10. Semicon defect PDPRP changes with time of voltage application; a, b, c, d and e correspond to ageing stages 1, 2, 3, 4, and 5 depicted in Fig. 9.

Initially in the first 500 hours the PDIV of the more severe defect (core 3) was on average, 25% smaller than that in the less severe defects (core 1 & 2). Such a behaviour is expected since the deeper the cut, the more is the stress enhancement and therefore less voltage required to initiate PD. Beyond 500 hours, the inception voltages became practically the same and this could be attributed to the changes in the discharge area due to continuous exposure to PD activity. PD magnitudes in the severe defect (core 3) were relatively bigger than in the less severe defects (core 1 & 2). In the latter however, after 500 hours, the magnitude reduced to near noise level. The PDPRPs of the ring-cut as depicted in Fig. 6 show that in both cases of defect severities, the overall 'turtle like' shape was maintained throughout the ageing period albeit with distinct changes in magnitude and repetition rates. The PD pulses occupy the first and third quarters of the voltage waveform and also extend into the zero crossing regions. Such a characteristic is manifestation of the influence of residual space charge in the discharge process; a signature of typical cavity discharges.

Tramline defect: As shown in Fig. 7 and Fig. 8, the more severe defect (core 3) has lower PDIV and bigger PD magnitudes than the less severe defects (core 1 & 2). The PDPRP begin as turtle shape but with ageing, change to 'rabbit ear' shape. As with the ring-cut defect, the PD magnitudes decrease significantly with time.

Semicon feather defect: With reference to Fig. 9 and Fig. 10, the more severe defect had more instances of PD evanescence compared to those in the less severe defects; this could be an indication of the semicon protrusion tip burnout. The sharper tip of the semicon feather would have caused more stress enhancement resulting in higher PD repetitions as shown in Fig. 10c. Consequently, the tip erodes much faster thereby reducing stress enhancement and eventually suppressing PD activity. The PDPRP show pulse position shifted more towards the supply peaks of the voltage waveform as characteristic of corona discharges. This behaviour is consistent with non-cavity discharges where the influence of residual space charge is minimal. Such a feature could be regarded as distinct for semicon feather defects.

In the next section a numerical model representing the physical changes in the discharge area during electrical ageing is implemented to reproduce discharge patterns similar to those measured.

III. COMPUTER SIMULATIONS OF PD MECHANISMS

There are various models available in the literature to simulate PD mechanisms. The 3-Capacitor model or commonly known as a-b-c model, initially introduced by Gemant and Philippoff in 1932 [13] is one that has been subsequently modified by various researchers to give reasonably accurate PD simulation results. In the present work, the 3-Capacitor model as modified by Haghjoo et al [14] is adopted to represent the cavity type defects (ring-cut and tramline) as well as the semicon feather defects in cable terminations.

A. The Modified 3-Capacitor PD Models

The concept of 3-Capacitor PD model emanates from the regions labelled a, b and c in Fig. 11 that effectively form three series capacitors. The labels in Fig. 11 are defined in Table 1. Using the dimensions, geometry and material properties of the sectorial region of interest as illustrated in Fig. 11, the equivalent circuit parameters can be deduced.

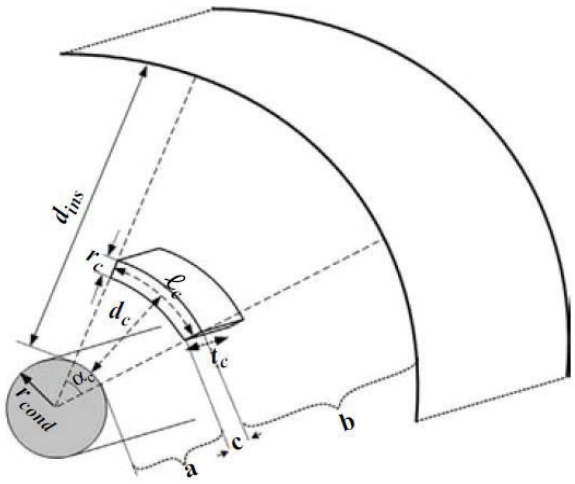

Fig. 11. Cross-section of a power cable containing a dielectric bound air-filled cavity [14]

TABLE I
DEFINITIONS OF SYMBOLS AND CORRESPONDING VALUES

Symbol	Definition
d_{ins}	Cable insulation thickness
r_{cond}	Cable core conductor radius
α_c	Defect sector angle
r_c	Cavity length
l_c	Cavity depth
t_c	Cavity width
a	Insulation portion between core and cavity
c	Sector occupied by cavity
b	Insulation portion between cavity and outer semicon
L	Cable test specimen length

The cable termination defects investigated in the present work as illustrated in Fig. 1 are located on the interface of the outer semicon and the insulation. It implies that the equivalent circuit reduces to that presented in Fig. 12 where the circuit parameters are analytically calculated using (1) to (10). The presence of a cavity in the insulation distorts the electric field distribution which inherently affects the capacitance and resistance parameters of the cavity itself and the adjacent insulation regions in the insulation sector. The corresponding equations for the capacitances and resistances incorporate the electric field distortion factors and thus is the essence of the modified 3-Capacitor model as derived in Haghjoo et al [14]. The symbols used in the equations are as defined in Fig. 11 and Table 1 and 2.

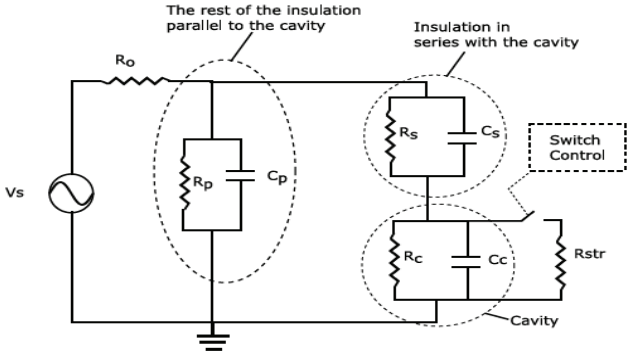

Fig. 12. The equivalent capacitive model of the insulation with an embedded air-filled cavity

$$C_a = \frac{\varepsilon_{ins}}{ln\left(\frac{\left(r_{cond}+d_{ins}-\frac{r_c}{2}\right)}{(r_{cond})}\right)} \cdot \frac{l_c}{r_{cond}+d_c} . t_c \quad (1)$$

$$C_b = \frac{\varepsilon_{ins}}{ln\left(\frac{(r_{cond}+d_{ins})}{\left(r_{cond}+d_{ins}+\frac{r_c}{2}\right)}\right)} \cdot \frac{l_c}{r_{cond}+d_c} . t_c \quad (2)$$

$$C_c = \frac{\varepsilon_0}{ln\left(\frac{\left(r_{cond}+d_{ins}+\frac{r_c}{2}\right)}{r_{cond}}\right)} \cdot \frac{l_c}{r_{cond}+d_c} . t_c \quad (3)$$

$$C_p = \frac{2\pi\varepsilon_{ins}}{ln\left(\frac{(r_{cond}+d_{ins})}{r_{cond}}\right)} . L \quad (4)$$

$$C_s = \frac{C_a C_b}{C_a+C_b} \quad (5)$$

$$R_a = \frac{1}{\sigma_{ins}} \frac{r_{cond}+d_c}{l_c t_c} ln\left(\frac{r_{cond}+d_c-\frac{r_c}{2}}{r_{cond}}\right) \quad (6)$$

$$R_b = \frac{1}{\sigma_{ins}} \frac{r_{cond}+d_c}{l_c t_c} ln\left(\frac{r_{cond}+d_{ins}}{r_{cond}+d_c+\frac{r_c}{2}}\right) \quad (7)$$

$$R_s = R_a + R_b \quad (8)$$

$$R_c = \frac{1}{\sigma_{surf}} \frac{r_{cond}+d_c}{l_c+t_c} ln\left(\frac{r_{cond}+d_c+\frac{r_c}{2}}{r_{cond}+d_c-\frac{r_c}{2}}\right) \quad (9)$$

$$R_p = \frac{1}{2\pi L\sigma_{ins}} ln\left(\frac{r_{cond}+d_{ins}}{r_{cond}}\right) \quad (10)$$

TABLE 2
SYMBOLS USED AND CORRESPONDING VALUES

Symbol	Definition	Value used in the simulation		
		Unaged	Moderately aged	Severely aged
σ_{ins}	Insulation conductivity	10^{-18} S	10^{-18} S	10^{-18} S
σ_{surf}	Cavity surface area conductivity	10^{-12} S	10^{-10} S	10^{-8} S
ε_0	Permittivity of free space	8.54×10^{-12} F·m^{-1}		
ε_{ins}	Insulation Relative permittivity	2.645		
R_{str}	Discharge arc resistance	108 Ω		

The PD measurement system depicted in Fig. 3 was simulated in Matlab Simulink™. The test object was the 1-meter long cable sample which translated to an equivalent circuit with parameters determined using the defect and cable dimensions. Other variables representing the physical process in a PD event such as a switch across the cavity and the random number function representing stochastic availability of the seed electron were also incorporated in the Simulink™ model. The values of the coupling capacitor and detection impedance were set to be equal to those in the actual physical circuit used in the PD measurements. The algorithm representing the discharge processes in Matlab Simulink™ is illustrated in Fig. 13.

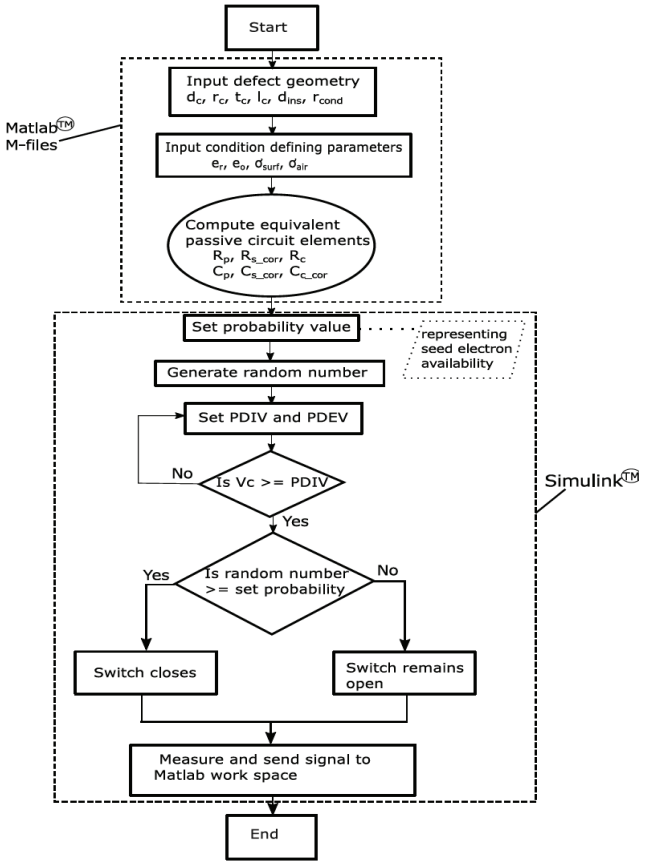

Fig. 13. The process flow of the PD model simulation algorithm

B. Simulation Results and Discussion

Ring-cut and Tramline (cavity type) PD defect: The virgin conditions are both characterised by setting the cavity surface resistance as high as possible; in the order of 10^{12} Ω. In the literature the measured surface conductivity ranges from 10^{-15}S at virgin stage, to 10^{-6} S for severely aged [11, 16]. The variations of the cavity defect shape as ring-cut or tramline were not accounted for in the simulations.

The voltage across the cavity at which the cavity breaks down (CPDIV) is a function of the gap overvoltage which is the difference between the intrinsic breakdown voltage and the actual breakdown voltage of the cavity [17]. The gap overvoltage in turn depends on the electro-chemical and physical conditions of the discharge area such as residual charge retention properties, gas pressure and gas composition [18, 19].

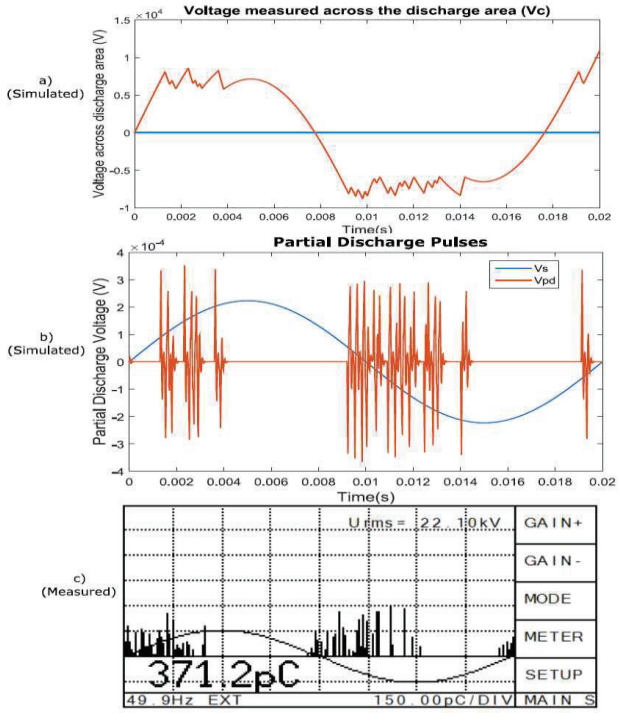

Fig. 14. PRPDP of the unaged cavity defect: a) Simulated voltage across the cavity, b) Detected voltage across the measuring impedance in the model, c) Typical similar measured pattern

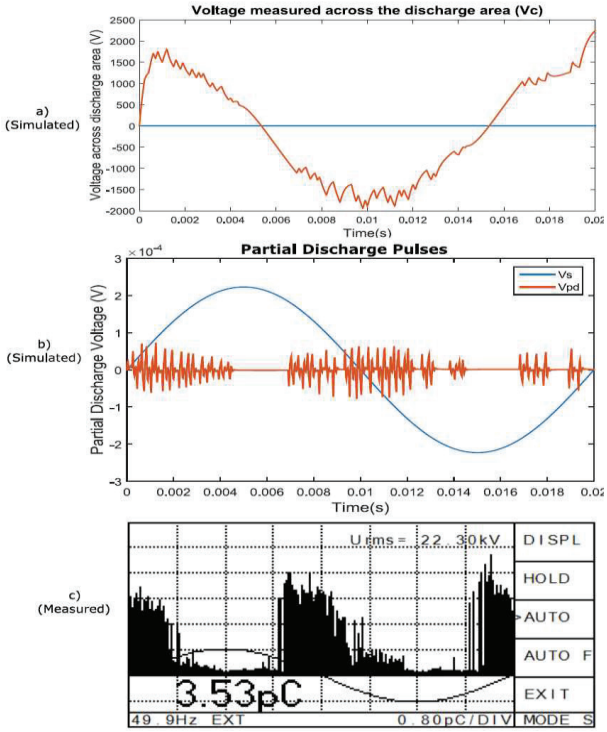

Fig. 15. PRPDP of the severely aged cavity defect: a) Simulated voltage across the cavity, b) Detected voltage across the measuring impedance in the model, c) Typical similar measured pattern

In virgin defects, the conditions favour higher gap overvoltage [17] and in the present model this situation is simulated by setting the CPDIV relatively high in the model; at 8 kV. The corresponding discharge extinction voltage is also set relatively high, at 6 kV. The simulated PD pulse phase-resolved patterns shown in Fig. 14 as measured voltage pulses show distribution patterns that are comparable to the actual physical measurements.

The severely aged conditions are characterised by setting the cavity surface conductance as relatively high as possible; in the order of 10^{-8} S. Due to the readily available seed electrons and micro-pits being consequences of erosion on the discharge surface due to continuous PD bombardment, there are localised stress enhancement resulting in much lower CPDIV [20]. In the model, the CPDIV was set at 1 kV and CPDEV at 0.5 kV. The resultant PDPRPs shown in Fig. 15 (both measured and simulated) are characterised by smaller PD pulses of higher repetition rate and with significant pulse presence in the zero crossing regions of the voltage waveform. At this stage the PD activity has high probability of transitioning into electrical treeing leading to imminent failure [20].

The semicon feather PD defect: The PRPDP of the semicon feather appeared with corona-like features with also partly surface discharges features. The equivalent circuit shown in Fig. 16 was used in the simulations. The insulation surface (represented by C_s and R_s) around the discharge spark tip becomes polluted with carbonaceous PD by-products. Consequently, the resistance becomes relatively small. In the simulations the resistance was set to 10^8 Ω and this produced PD pulses similar to the measured patterns as shown in Fig. 17.

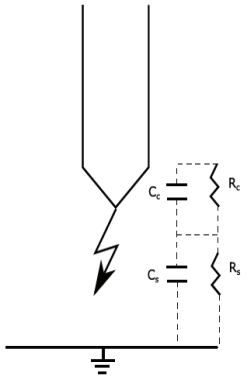

Fig. 16. The equivalent circuit of the Semicon feather defect

TABLE 3
SEMICON FEATHER EQUIVALENT CIRCUIT SYMBOLS AND DEFINITIONS

Symbol	Definition
C_c	Equivalent capacitance of the region in front of the semicon tip that is short circuited by the discharge arc
R_c	Equivalent resistance of the region in front of the semicon tip that is short circuited by the discharge arc
C_s	Equivalent capacitance of between the tip of discharge arc and the opposite grounded electrode
R_s	Equivalent resistance of between the tip of discharge arc and the opposite grounded electrode

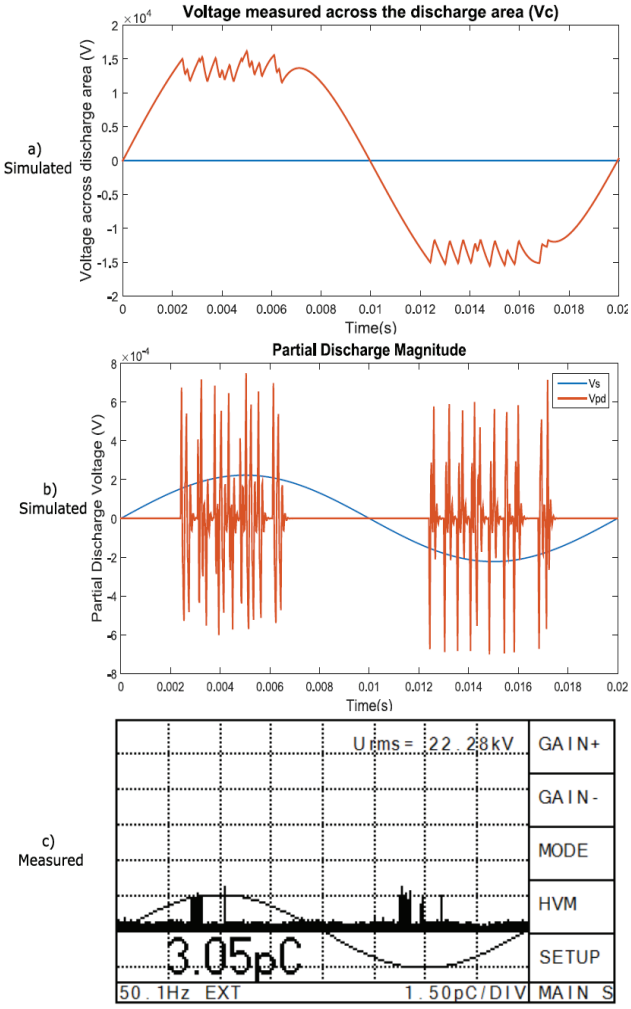

Fig. 17. PRPDP of the semicon feather defect PD

IV. Conclusion

The time-evolution of PD parameters in typical installation defects of MV XLPE cable terminations have been studied through physical measurements. The PDPRP, PDIV and apparent charge magnitudes were found to evolve in a specific way depending on the defect types. The PD behaviour was interpreted by comparison with computer numerical simulation results.

The 3-Capacitor model that is modified to incorporate stress enhancements in the cavity and adjacent insulation regions was used in the simulations. The physical changes in the discharge defect that occur due to continuous PD activity were simulated through varying the discharge surface conductivity as well as the discharge gap inception and extinction voltages. The defect type distinct time-evolution changes in the partial discharge phase-resolved patterns were reproduced through the simulations.

The ability to recognise power cable termination defect type through PD tests immediately after installation as well as during the course of on-line PD monitoring is valuable. The knowledge strengthens the credibility of PD diagnosis as a commissioning test as well as in-service condition monitoring technology of MV power cable terminations.

References

[1] I. Pérez-Arriaga and C. Knittel, “Utility of the Future - An MIT Energy Initiative response to an industry in transition,” Massachusetts Institute of Technology (MIT), Boston, USA, Dec. 2016. [Online]. Available: energy.mit.edu/uof

[2] W. Vahlstrom, “Strategies for field testing medium voltage cables,” IEEE Elect. Ins. Magazine, vol. 25, pp. 1-17, Oct. 2009.

[3] H. E. Orton, “Diagnostic testing of in-situ power cables-An overview,” IEEE/PES Trans. Distrib. Conf. Exhib., Asia Pacific, vol. 3, pp. 1420–1425, 2002.

[4] S. M. Gargari, P.A.A.F. Wouters, P.C.J.M. van der Wielen, and E. F. Steennis, “Practical Experiences with On-line PD Monitoring and Interpretation for MV Cable Systems,” in Proc. International Conference on Solid Dielectrics, Potsdam, Germany, July 2010.

[5] IEEE Guide for Field Testing and Evaluation of the Insulation of Shielded Power Cable Systems Rated 5 kV and Above, IEEE Standard 400, 2012.

[6] D. Pepper, “PD-measurements on typical defects on XLPE-insulated cables at variable frequencies,” in Proc. of the 10th Int. Symp. in HV Eng. (ISH), Montreal, Canada, 1997.

[7] D. Fynes-Clinton and C. Nyamupangedengu, “Partial Discharge Characterization of Cross-Linked Polyethylene Medium Voltage Power Cable Termination Defects at Very Low Frequency (0.1 Hz) and Power Frequency Test Voltages,” IEEE Elect. Ins. Magazine, vol. 32, no. 4, pp. 16-23, July/August 2016.

[8] G. Mazzanti and G. C. Montanari, “A comparison between XLPE and EPR as insulating materials for HV cables,” IEEE Trans. on Power Delivery, vol. 12, no. 1, pp. 15–26, 1997.

[9] M. S. Mashikian and A. Szatkowski, “Medium voltage cable defects revealed by off-line partial discharge testing at power frequency,” IEEE Elect. Ins. Magazine, vol. 22, no. 4, pp. 24–32, 2006.

[10] R. Bartnikas, R. J. Densley, and R. M. Eichhorn, “Long term accelerated aging tests on distribution cables under wet conditions,” IEEE Trans. on Power Delivery, vol. 11, no. 4, pp. 1695–1699, 1996.

[11] R. Bartnikas, H. Doepken, G. Eichhorn, G. Rittmann, and W. Wilkens, “Accelerated Life Testing of Wet Cable Specimens at Frequencies above 60 Hz,” IEEE Trans. on Power App. and Syst., vol. PAS-99, no. 4, pp. 1575–1585,1980.

[12] IEC High Voltage Test Techniques - Partial Discharge Measurements, IEC Standard 60270, 2000.

[13] Z. Achillides, G. Georghiou, and E. Kyriakides: “Partial discharges and associated transients: The induced charge concept versus capacitive modelling”, IEEE Trans. on Dielectrics and Elect. Ins., vol. 15, no. 6, pp. 1507-1516, 2008.

[14] F. Haghjoo, E. Khanahmadloo, and S. Shahrtash, “Comprehensive 3-capacitors model for partial discharge in power cables”, International Journal for Computation and Mathematics in Electrical and Electronic Engineering, vol. 31, no. 2, pp. 346-368, 2012.

[15] K. Temmen, “Evaluation of surface changes in at cavities due to ageing by means of phase-angle resolved partial discharge measurement”, Journal of Physics D: Applied Physics, vol. 33, no. 6, pp. 603-608, 2000, 10.1088/0022-3727/33/6/303

[16] P. V. Glahn, R. Van Brunt, and T. Las, “Nonstationary behaviour of partial discharge during discharge induced ageing of dielectrics”, in IEE Proc. -Science Measurement Technology, vol. 124, 1995, pp. 37-45.

[17] R. Bartnikas and J.P. Novak, “Effect of overvoltages on the rise time and amplitude of PD pulses”, IEEE Trans. on Dielectric Elect. Ins., vol. 2, pp. 557-566, 1995.

[18] J. C. Devins, “The physics of partial discharges in solid dielectrics”, IEEE Trans. on Elect. Ins., vol. EI-19, no. 5, pp. 475-495, 1984.

[19] F. Gutfleisch, “Measurement and Simulation of PD in Epoxy Voids," IEEE Trans. on Dielectrics and Elect. Ins., vol. 2, no. 5, pp. 729-743, 1995.

[20] P. Morshuis, “Assessment of dielectric degradation by ultrawide-band PD detection”, IEEE Trans. on Dielectrics and Elect. Ins., vol. 2, no. 5, pp. 744-760, 1995

E. N. N. Haikali was born in Namibia. She holds a bachelor's degree with honours in Electrical Engineering from the University of Namibia and recently completed a Master's Degree with the University of the Witwatersrand in South Africa. Her work focuses on High Voltage Insulation Condition Monitoring and Assessment with the purpose of improving insulation diagnosis. She is now an Assistant Engineer at NamPower, a power utility company in Namibia.

C. Nyamupangedengu was born in Zimbabwe. He received his bachelor's degree with honours in electrical engineering from the University of Zimbabwe in 1994. He received his MSc (with distinction) and PhD at the University of the Witwatersrand in 2004 and 2011 respectively. His early work experience includes being an engineer at Zimbabwe Electricity Supply in power system planning and development. He is currently an Associate Professor of High Voltage Engineering at the University of the Witwatersrand. His passion and expertise is in the research on the diagnosis of high voltage insulation. He served as Cigre SC D1 (Materials and emerging test techniques) representative of the Cigre Southern Africa. He is an active member of the Cigre WG D1-50 (Atmospheric and altitude correction factors for air gaps and clean insulators) and D1-61 (Optical corona detection and measurement).